Open access • Journal Article • DOI:10.1016/0168-9002(94)01465-5

# The SLAC high-density gaseous polarized 3He target☆ — Source link

J.R. Johnson, Alan K. Thompson, T. E. Chupp, Timothy B. Smith ...+6 more authors

**Institutions:** University of Wisconsin-Madison, Harvard University, University of Michigan, Princeton University ...+1 more institutions

**Published on:** 01 Mar 1995 - Nuclear Instruments & Methods in Physics Research Section A-accelerators Spectrometers Detectors and Associated Equipment (North-Holland)

**Topics:** Linear particle accelerator

# THE SLAC HIGH–DENSITY GASEOUS POLARIZED $^3$He TARGET*

J. R. Johnson
Department of Physics, University of Wisconsin, Madison, WI 53706

A. K. Thompson
Department of Physics, Harvard University, Cambridge, MA 02138

T. E. Chupp and T. B. Smith
Randall Laboratory of Physics, University of Michigan, Ann Arbor, MI 48109

G. D. Cates, B. Driehuys, H. Middleton, and N. R. Newbury
Joseph Henry Laboratories of Physics, Princeton University, Princeton, NJ 08544

E. W. Hughes and W. Meyer*
Stanford Linear Accelerator Center, Stanford University, Stanford, CA 94309

## ABSTRACT

A large-scale high-pressure gaseous $^3$He polarized target has been developed for use with a high-intensity polarized electron beam at the Stanford Linear Accelerator Center. This target was used successfully in an experiment to study the spin structure of the neutron. The target provided an areal density of about $7\times10^{21}$ nuclei/cm$^2$ and operated at $^3$He polarizations between about 30% and 40% for the six-week duration of the experiment.

---

*Work supported in part by Department of Energy contracts DE–AC03–76SF00515 (SLAC), DE–FG02–90ER40557 (Princeton), and DE–AC02–76ER00881 (Wisconsin); by National Science Foundation grants 8914353 and 9200621 (Michigan); and by the Bundesministerium für Forschung und Technologie (W. Meyer).

*Permanent address: Universität Bonn, Bonn, Germany.

## INTRODUCTION

Experiment E-142 at SLAC [1] was proposed to measure the spin-dependent structure function of the neutron by studying deep-inelastic scattering of high-energy polarized electrons from polarized neutrons. Polarized $^3$He was chosen as the target material to provide the polarized neutrons for two main reasons. First, $^3$He nuclear wave-function calculations [2] indicate that the nucleus is primarily in a spatially symmetric S-state where the spins of the two protons must be anti-aligned. Thus the spin of the nucleus is mainly provided by the neutron, and so polarized $^3$He is a good approximation to a polarized neutron target, diluted by the presence of the protons but with only small corrections needed due to the polarization of the protons. Second, practical $^3$He polarized targets have been developed [3–10] using the technique of collisional spin-exchange with optically pumped alkali-metal vapor, typically rubidium. Using modern high-power Ti:sapphire lasers for the depopulation optical pumping of rubidium, such targets have been shown to be capable of operating effectively at high $^3$He pressures (more than 10 atm [8]) and in the presence of intense electron beams [10], as required by the SLAC experiment. A disadvantage of this technique is the weakness of the hyperfine interaction between the polarized rubidium valence electron and the $^3$He nucleus, leading to typical time constants for the build-up of $^3$He polarization of the order of 10 hours. Thus, long $^3$He spin relaxation times are required to achieve high polarization.

## TARGET DESCRIPTION

Figure 1 shows a schematic overview of the SLAC target system. The large main Helmholtz coils have a diameter of about 1.5 m and provide a uniform magnetic field of about 20 G in the vicinity of the target cell during operation. The coils shown produced a field direction parallel (or antiparallel) to the electron beam direction, and this direction (and thus the direction of the $^3$He polarization) was reversed every few hours during

the experiment. Not shown is a second set of coils that produced a magnetic field (and $^3$He polarization) direction transverse to the beam direction for part of the experiment. The RF drive coils are about 50 cm in diameter and, together with the small pickup coils shown, were used for NMR measurements of the $^3$He polarization, as described later in this paper.

The laser shown in the figure represents one of five Ti:sapphire lasers, each pumped by a 20 W argon-ion laser and capable of delivering several watts of power at 795 nm, the wavelength of the $D_1$ line of rubidium. Together, the five laser systems typically produced nearly 20 W of infrared photons for optical pumping. The quarter-wave plate in each laser beam line was adjusted to produce circularly polarized photons, and the mirrors shown were oriented so as to preserve the circular polarization.

As indicated in fig. 1, the $^3$He gas was contained in a sealed glass vessel constructed as two chambers connected by a transfer tube, for reasons discussed below. The chamber in the electron beam was a cylinder about 2.1 cm in diameter and 30 cm long, with end windows about 125 μm thick. The other chamber was about 3.7 cm diameter by 8 cm long, and was enclosed in a plastic oven connected to hot air supply and return tubes (not shown). The oven had an optically coated laser-beam entrance window on one end, and transparent plastic windows on two adjacent sides to allow observation of the rubidium fluorescence during optimization of laser steering and wavelength adjustment. The oven was operated typically at about 175˚C, giving a typical rubidium vapor density of a few times $10^{14}$ atoms/cm$^3$ and a $^3$He pressure in the sealed vessel of about 11 atm.

The target cell, oven, and NMR coils were required to operate in a completely evacuated beam line, to minimize backgrounds and unpolarized material intercepting the electron beam. The oven and the support structure for the NMR coils and target cell were constructed of plastic or other nonconducting material, to avoid disrupting the RF drive

field during NMR measurements. The entire target structure was constructed of nonmagnetic materials so as not to degrade the uniformity of the main holding field.

## TARGET DESIGN CONSIDERATIONS

### THE TWO-CHAMBER CELL

One requirement of the target arrangement was that the optical pumping of the rubidium vapor take place away from the electron beam, since the rubidium would be depolarized through ionization by the intense beam. In principle, a single cylindrical chamber could be pumped in a location outside the experimental area, then installed in the beam line to replace another cell when the polarization of the latter has dropped too low. However, in the SLAC environment, a long access time would be required to secure the experimental area, break the beam-line vacuum, exchange the target cells, then restore the vacuum, and finally retune the accelerator. Also, the glass cell walls could darken from radiation damage and prevent repumping of the cell, the target polarization would be varying at all times, recovery time from an accidental loss of polarization could be very long, and the pressure (and hence stress) while pumping would be substantially higher for the same operating pressure in the cell. The "double cell" solves or minimizes these problems, and in principle one good cell of this design could operate for the whole experiment. In this design, the $^3$He is polarized in the upper (pumping) chamber and diffuses through the transfer tube to the lower (target) chamber with a time constant of about 10 min—small compared with the characteristic spin exchange and relaxation times. Due to the low thermal conductivity of glass, the target chamber remains at a low enough temperature (about 60°C) that the rubidium vapor density there is negligible. The disadvantage of this design is that the effective spin-exchange time is increased, and the cell is more difficult to construct.

## MAXIMIZING POLARIZATION

The asymptotic $^3$He polarization is given by $P_{^3He} = (\gamma_{SE}/\gamma_{SE}+\Gamma) \langle P_{Rb} \rangle$, where $\gamma_{SE}$ is the spin-exchange rate between the rubidium and the $^3$He, $\Gamma$ is the $^3$He spin relaxation rate due to all other effects, and $\langle P_{Rb} \rangle$ is the average rubidium polarization. If adequate laser power reaches all parts of the pumping chamber, $\langle P_{Rb} \rangle$ can approach 100%. Since $\gamma_{SE}$ is proportional to the rubidium number density, this term may be increased by increasing the oven temperature to vaporize more rubidium, but then more laser power is needed to maintain $\langle P_{Rb} \rangle$. Practical limitations are then reached due to the cost and complexity of more lasers, or to the temperature limits of the oven materials, or both. The remaining variable is then the spin relaxation rate $\Gamma$, which should be minimized.

## RELAXATION EFFECTS

The total $^3$He spin relaxation rate is the result of several effects, here approximately $\Gamma = \Gamma_{bulk} + \Gamma_{beam} + \Gamma_{field} + \Gamma_{gas} + \Gamma_{wall}$, as identified below. The first two of these are unavoidable. **BULK** relaxation results from $^3$He–$^3$He collisions, where a dipolar interaction couples the nuclear spin to the orbital angular momentum of the colliding atoms. At a pressure of about 10 atm, this limits the relaxation time to approximately 75 hours. **BEAM** depolarization results from ionization and recombination of $^3$He exposed to an electron beam. This was not a major effect during much of the experiment, but caused a noticeable (several percent) reduction in target polarization at the highest beam currents (about 4 μA).

The remaining terms are ones over which the target builders have some control. Magnetic **FIELD** inhomogeneities induce depolarization as the $^3$He atoms diffuse throughout the cell volume. The solution for this target was to use large Helmholtz coils to produce the holding field, as such a design was required in any case to provide access to the target vacuum chamber. The last two effects listed are due to collisions of $^3$He atoms

with paramagnetic impurities in the **GAS** mixture, and collisions with the cell **WALLS**. These relaxation effects can be minimized by careful attention to details of cell production, as discussed below.

## CELL MANUFACTURE

Figure 2 shows a diagram of the system used for preparing and filling target cells. The cell is connected to a high-vacuum system capable of $10^{-8}$ Torr, and baked under vacuum for up to 7 days at 450˚C. A small amount of rubidium is then "chased" into the pumping chamber with a torch, and the target chamber is inclosed in a vacuum-walled enclosure through which liquid $^4$He is blown. A small amount of 99.9995% pure nitrogen is introduced into the cell (this suppresses "radiation trapping" in the optical pumping process [7]) and the desired amount of high-purity $^3$He s flowed through a liquid $^4$He trap into a calibrated volume, then introduced into the cell. The temperature of the target chamber is lowered enough (by the liquid $^4$He blowing by) to reach a pressure below atmospheric, and the small entrance tube at the top of the pumping chamber is then sealed with a torch.

The construction of the cell itself is also critical for achieving long relaxation times. Aluminosilicate glass has been found to highly suitable for this purpose, possibly due to its relatively low porosity to $^3$He. For the cells used in this experiment, commercial tubing (Corning 1720) was rinsed with nitric acid to remove possible surface contaminants, then reblown to the desired dimensions on a glass-working lathe, resulting in a very clean and microscopically smooth "fire-polished" surface. Cells constructed in this manner and filled as described above were measured to have net relaxation times up to 65 hours at room temperature with no incident electron beam, or nearly the bulk limit.

## POLARIZATION MEASUREMENT

The method chosen for measuring target polarization was the NMR technique called Adiabatic Fast Passage, or AFP. This technique is relatively well-understood, had been used successfully in earlier work with similar targets, and was compatible with the experimental arrangement of this target. Figure 3 shows a diagram of the apparatus used for the measurement. An RF drive field orthogonal to the main field is applied at a fixed frequency of 92 kHz, while the main holding field strength is varied from the normal value of 20 G to a maximum of 38 G , passing through resonance for $^3$He at this frequency when the field is about 29 G . If the strength of the drive field and the rate of change of the main field strength are chosen correctly, essentially all of the $^3$He nuclear spins flip over during this process and the target polarization ends up reversed. The precessing nuclear spins induce a signal in the small pickup coils. This signal passes through a preamplifier in such a way as to cancel common-mode noise, and is transmitted to a lock-in amplifier locked to the frequency of the drive field. An adjustable circuit ("A-$\phi$ Box") produces a signal used to cancel any direct pickup from the drive field. Figure 4(a) shows a typical $^3$He signal resulting from this procedure. The main field is then swept back to the normal value, reversing the process and restoring the polarization to the direction being pumped, while providing another measurement of the $^3$He signal. Repeated measurements show that very little polarization ($< 0.1\%$) is lost in this procedure.

The method is calibrated by replacing the $^3$He cell with a nearly identical cell filled with distilled water, then performing repeated measurements with the same apparatus at the same frequency. The calculable thermal equilibrium polarization of the protons in the water is very small (about $10^{-8}$) at such low magnetic fields (at 92 kHz, protons are resonant at about 22 G ), but the density in water is high enough to create measurable signals during AFP (less than 2 $\mu$V in this setup). Many measurements must be averaged to achieve

acceptable signal-to-noise ratio, and the process is very time-consuming because the proton spin relaxation time in distilled water is about 2 s, so a substantial waiting time is required between sweeps in either direction. Figure 4(b) shows the average of 25 proton signals from a typical water measurement.

Experimental errors in the polarization measurement can arise from several sources. The largest contribution for this experiment was from the extraction of the proton signal from water measurements, with an estimated uncertainty of ±5.6%. The $^3$He density in the target chamber was determined from measurements made during cell filling, and from temperature measurements of the two chambers of the cell during operation, and contributes an estimated uncertainty of ±2.5%. Uncertainty in measurement of the diameter of the reblown tubing for the target chamber introduces another 2.6% error. When these are combined with several less significant effects, the overall uncertainty in the $^3$He polarization during this experiment is estimated to be ±7%, which is small compared with the statistical errors in the results of the experiment.

## OPERATIONAL EXPERIENCE

Figure 5 shows the measured $^3$He polarization as a function of time during the six-week experimental run. The polarization was generally maintained between about 30 and 40%, with variations primarily due to certain episodes indicated by arrows on the figure.

(1) The first (and best) cell installed had to be removed when the plastic oven cracked and leaked due to prolonged exposure to high temperature while surrounded by vacuum. (This cell was reinstalled later with a replacement oven and finished the experiment).

(2) The next cell had insufficient rubidium metal in the pumping chamber, and had to be removed when all the rubidium metal had migrated to the transfer tube and the rubidium vapor density dropped too low.

(3) The next cell behaved in a way that at first appeared similar to the second cell, but instead can be attributed to a leak of $^3$He, possibly due to slightly different cell construction. The evidence is that the electron scattering rates dropped linearly with the $^3$He NMR signals during this episode, implying a decrease in $^3$He density rather than polarization.

(4) Some time was spent running with target polarization oriented transverse to the beam direction. The arrangement was not capable of optical pumping in this orientation, so the polarization decayed until the longitudinal orientation was restored. For the transverse running, the main holding field was provided by a second set of Helmholtz coils, as mentioned earlier.

(5) Near the end of the experiment the beam intensity was increased, leading to additional depolarization due to ionization by the electrons.

In general, this target performed quite well considering the large size and complexity of the device compared with earlier experiments. For future running, several improvements are anticipated. Using better plastics for the oven will improve reliability and allow somewhat higher average temperatures, leading to greater rubidium vapor density and hence reduced spin-exchange times. Improvements will be made to the laser beam transport optics to increase the amount of laser power that reaches the rubidium vapor. This will increase the average rubidium polarization, or maintain it in the face of higher rubidium density. Finally, with more experience in cell construction, it is expected that cells will be produced that are longer, at higher $^3$He pressure, and with substantially thinner end windows, thus greatly increasing the fraction of polarizable material exposed to the electron beam.

## REFERENCES


[1] P. L. Anthony et al., Phys. Rev. Lett. 71 (1993) 959.

[2] R. M. Woloshyn, Nucl. Phys. 496A (1989) 749.

[3] M. A. Bouchiat, T. R. Carver, and C. M. Varnum, Phys. Rev. Lett. 5 (1960) 373.

[4] R. L. Gamblin and T. R. Carver, Phys Rev. 138 (1965) 964.

[5] N. D. Bhaskar, W. Happer, and T. McClelland, Phys. Rev. Lett. 49 (1982) 25.

[6] W. Happer et al., Phys. Rev. A29 (1984) 3092; Phys. Rev. A31 (1985) 260.

[7] T. E. Chupp et al., Phys. Rev. C36 (1987) 2244.

[8] B. Larson et al., Phys. Rev. A44 (1991) 3108; Phys. Rev. Lett. 67 (1991) 3356.

[9] N. R. Newbury et al., Phys. Rev. Lett. 67 (1991) 3219;
Phys. Rev. Lett. 69 (1992) 391.

[10] T. E. Chupp et al., Phys. Rev. C45 (1992) 915.

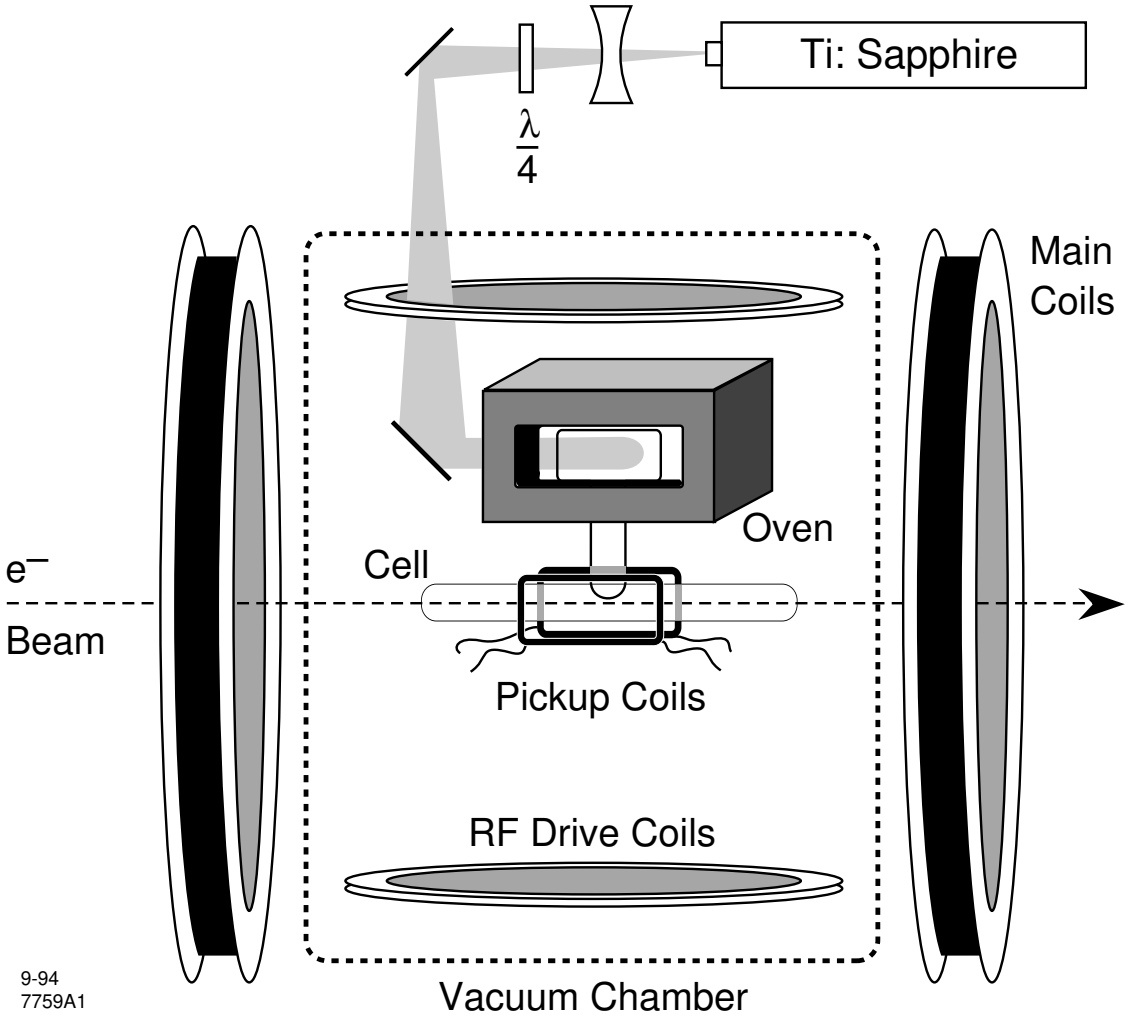


Fig. 1. Schematic overview of the SLAC $^3$He polarized target. Not shown are four of five identical Ti:sapphire lasers, the argon-ion lasers used to pump the Ti:sapphire, and the optics used to combine the five laser beams. Also not shown is a second set of main magnet coils with an axis transverse to the electron beam direction.

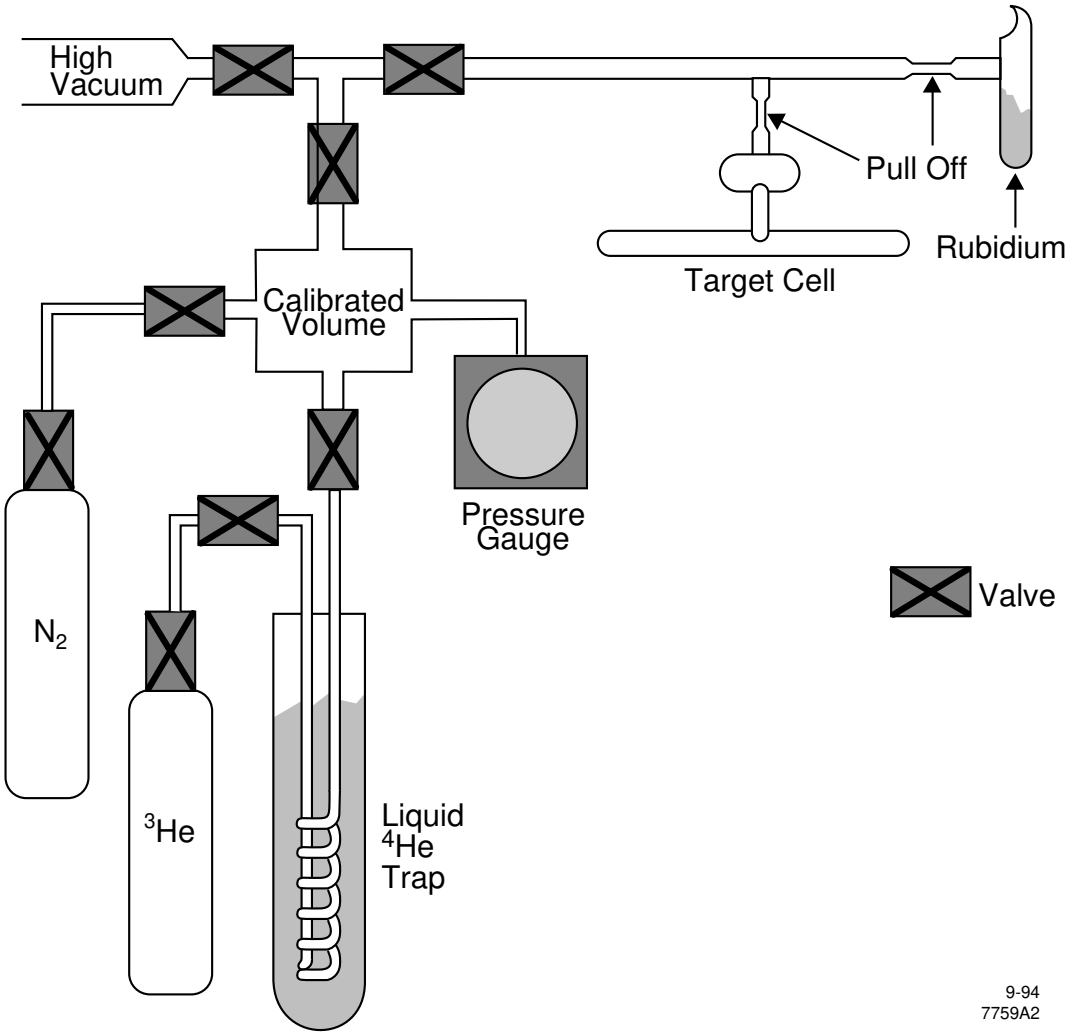


Fig. 2. Schematic diagram of the vacuum and gas filling system used for preparing target cells. Not shown is a vacuum jacket placed around the lower chamber of the cell while cooling with liquid helium.

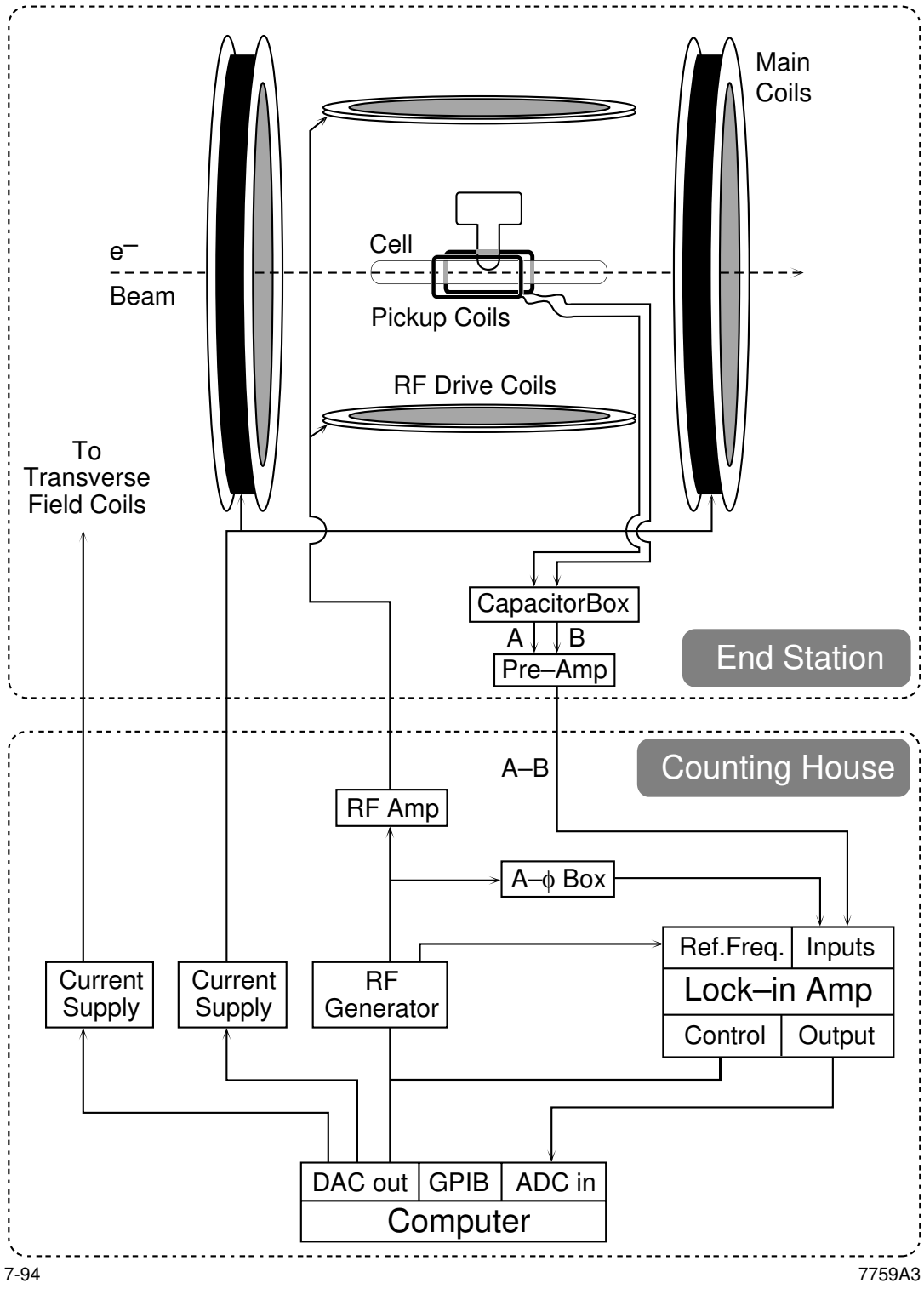


Fig. 3 Schematic diagram of the apparatus used for Adiabatic Fast Passage NMR measurements of the target polarization.

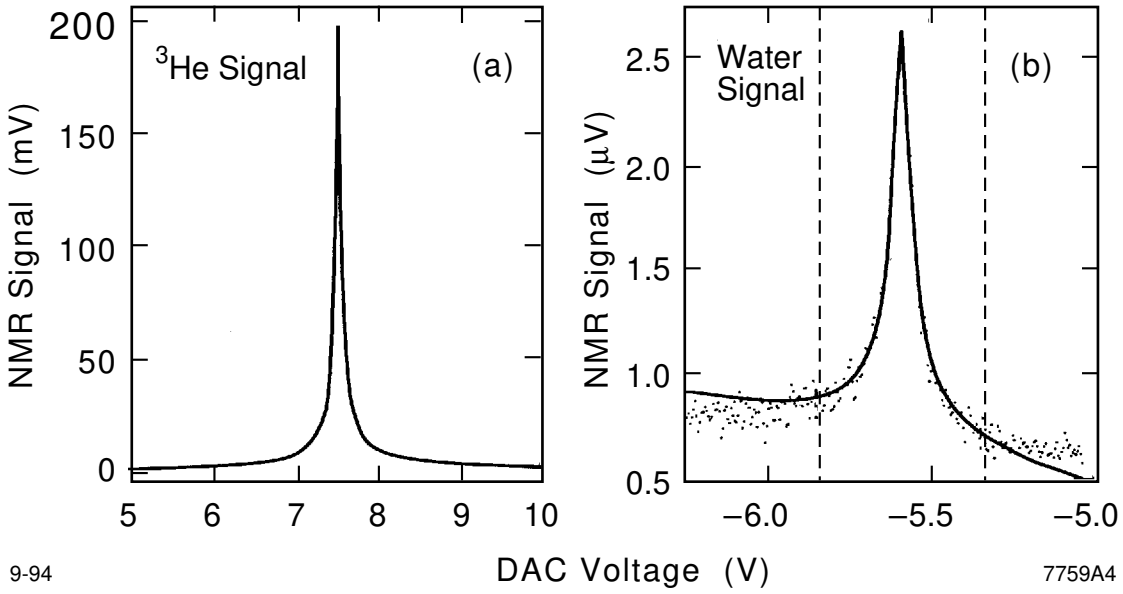


Fig. 4. (a) Typical NMR signal from the lock-in amplifier during an AFP measurement with polarized $^3$He. The solid line is a fit to a theoretical line shape and cannot be distinguished from the individual data points.

(b) Typical AFP signal from a water-filled calibration cell. The data points are averaged over 25 individual measurements. The solid line is a fit to a theoretical line shape with a linearly varying background. The dashed lines indicate the limits of the fit region.

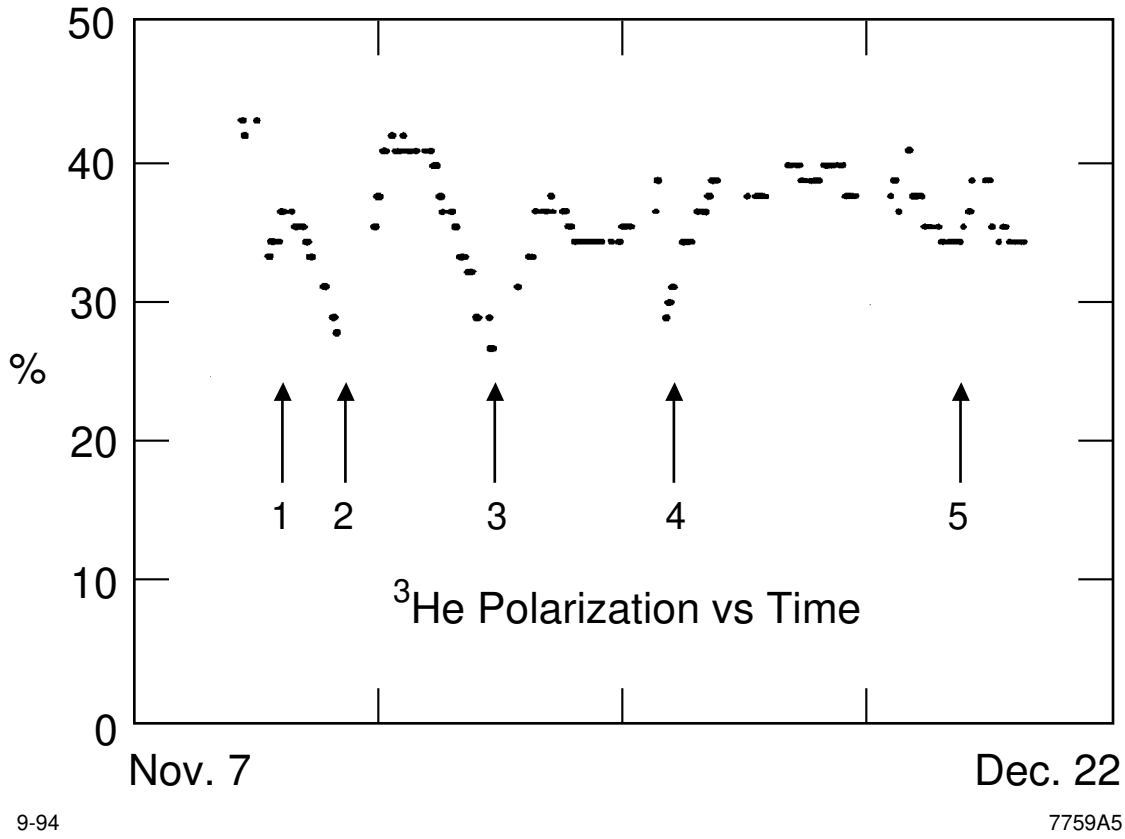


Fig. 5. Time dependence of on-line $^3$He polarization measurements during the course of the experiment. Numbered arrows indicate episodes discussed in the text.